Upgrading the AZT24 telescope at the Campo Imperatore high-altitude observatory: design and installation of a new, seeing-enhanced NIR imager

M. Dolci[*,a], E. Brocato[a], G. Rodeghiero[b], S. Di Frischia[a], P. D'Incecco[a], M. Canzari[a], S. Benedetti[a], F. De Luise[a], M. Di Carlo[a], A. Di Cianno[a], N. Napoleone[a], A. M. Piersimoni[a], E. Portaluri[a], G. Raimondo[a], L. Tartaglia[a], A. Valentini[a], G. Valentini[a]
[a]INAF – Osservatorio Astronomico d'Abruzzo, Via Maggini snc, 64100 Teramo (ITALY);
[b]INAF – Osservatorio di Astrofisica e Scienza dello Spazio, Via Gobetti 93/3, 40129 Bologna (ITALY)

ABSTRACT

The AZT24 is a 1.1m telescope installed at the Campo Imperatore observing station, in Central Italy, at an elevation of 2200 m a.s.l. Since the 2nd half of 1990s, its focal plane has been equipped with SWIRCAM, a 1-2.5 micron camera based on an LN2-cooled, HgCdTe detector, able to exploit the excellent observing conditions offered by the site, especially at those wavelengths.

After almost 30 years of operation, this system will now be upgraded with a new IR imager, based on an InGaAs detector, TEC-cooled at around -80 °C. Even with a reduced spectral coverage, the NIR imager will cover a wider field-of-view and will benefit from the seeing-enhancement capability produced by a devoted Tip-Tilt (TT) corrector.

The overall project is presented in this paper, with emphasis on a commercial InGaAs detector for astronomical applications. The opto-mechanical layout is optimized to reduce the instrumental thermal background, while the TT-correction system produces a significant narrowing of the PSF, increasing the signal-to-noise ratio of the detected sources. Simulations of the expected performances are reported: they show that the upgraded system is suitable for a number of science cases, ranging from extragalactic Astronomy to stellar Astrophysics and Solar System studies. In addition, it represents an interesting testbench for some technological investigations, both in the field of Adaptive Optics and in that of data acquisition and processing techniques.

Keywords: Near-infrared, cameras, tip-tilt correction, small telescopes

1. INTRODUCTION

Near-infrared astronomy has revolutionized our understanding of the universe. At these wavelengths (1 – 2.5 μm) light can penetrate dust clouds and reveal structures and processes that are heavily obscured at visible wavelengths, as in star-forming regions, proto-stars with their protoplanetary disks and the central regions of the galaxies, including the Milky Way. In addition to that, the observation of the infrared spectrum has opened to a wide variety of astrophysical science cases, from the study of molecular species in stellar atmospheres and interstellar clouds, to the properties of cold ($T < 2000$ K) clouds and stellar atmospheres, to the reddening caused by the cosmological redshift.

Despite the challenges posed by atmospheric absorption and emission - which have been completely overcome by space-based observatories only - ground-based infrared observations still play a crucial role, also representing a vital complement to space-based observations, thanks to the continuous technological advancements in the field of instrumentation, as well as to the continuous development of observational and data processing techniques.

*mauro.dolci@inaf.it; phone 39 0861 439705

Ground-based and Airborne Instrumentation for Astronomy X, edited by Julia J. Bryant, Kentaro Motohara, Joël R. D. Vernet, Proc. of SPIE Vol. 13096, 130968W
© 2024 SPIE · 0277-786X · doi: 10.1117/12.3020225

Modern infrared imaging detectors [1] have significantly enhanced our ability to capture and analyze radiation from the cosmic sources. Their evolution has been marked by several key technological advancements, in particular the development of CMOS sensors, deeply cooled to reduce thermal noise and based on materials especially sensitive to infrared radiation, like mercury cadmium telluride (HgCdTe) and indium antimonide (InSb). In recent years, Indium Gallium Arsenide (InGaAs) detectors emerged significantly due to their superior sensitivity and performance in the near-infrared range between 0.9 and 1.7 μm. Improvements in material quality, detector design, and readout electronics have led to significant enhancements in performance, including better noise characteristics and higher dynamic range, attracting growing interest in their use in astronomical observations [2][3][4].

Other key developments have pushed ground-based infrared astronomy forward: among these, Adaptive Optics systems have revolutionized our ability to counteract the blurring effects of the Earth's atmosphere, providing sharper images and higher S/N data. Nowadays, large telescopes equipped with infrared instruments, such as the Very Large Telescope (VLT), take advantage of advanced Adaptive Optics systems which exploit wavefront sensing at visible wavelengths to perform adaptive correction in the near-infrared range.

In this paper we present the project for the refurbishment of the infrared facility at the Campo Imperatore Observatory, a remote observing station of the INAF-Abruzzo Astronomical Observatory, located at an elevation of 2200 m a.sl. on the Central Italy Appennino. The site is characterized by excellent observing conditions at near-infrared wavelengths, thanks to the cold and dry atmosphere (Figure 1).

The project, based on *NextGenerationEU funding program*, aims at: 1) installing a new, large format InGaAs imaging detector as a replacement of the old SWIRCAM camera; 2) simplifying the management system by replacing the cryogenic cooling with a thermoelectric one; and 3) exploiting the power of a tip/tilt correction offered by advanced wavefront sensors and piezoelectric devices, now commercially available. The new instrument has been named CI^{2}RCE (Campo Imperatore InfraRed Camera with seeing Enhancer).

The ideas behind the refurbishment concept are shown in Section 2, which also highlights the opportunity offered by the National Recovery and Resilience Plan (Piano Nazionale di Ripresa e Resilienza, PNRR) of the Italian Government, based on the NextGenerationEU fuding program. Section 3 reports the current status of the opto-mechanical layout, including the infrared detector and the tip/tilt correction system, while simulations of the expected sensitivity are described in Section 4. The last two Sections (5-6) are devoted to a number of science cases that could be pursued with CI^{2}RCE and a short summary of the next program milestones.



Figure 1. A spectacular view of the Campo Imperatore Observatory during the deep winter. This cold and dry site offers excellent observing conditions for astronomical observations at near-infrared wavelengths.

2. REFURBISHMENT IDEAS AND OPPORTUNITY: THE CI²RCE CONCEPT

The AZT24 telescope is a 1.1 m, f/7.2 Ritchey-Chretien reflector, whose focal plane has been equipped with the near-infrared camera SWIRCAM in 1996 [5]. SWIRCAM is based on a 256x256 HgCdTe PICNIC detector sensitive in the 0.9 - 2.3 μm wavelength range, with a pixel size 40 μm: each single acquired image covers therefore a Field-of-View of 4.4 x 4.4 arcmin^2 with a platescale of 1.04 arcsec/pixel. SWIRCAM hosts broad-band Johnson J,H,K,K' filters plus a number of narrow-band filters for astronomical imaging, and two grisms for low-resolution (about 220) spectroscopy in the I+J and H+K regions. Detector, optics and filter and grism wheels work in a high-vacuum, cryogenic environment cooled at 77 K inside a LN2 dewar built by IRLabs, Inc.

The AZT24+SWIRCAM system worked until 2016, producing astronomical data mainly concerning the SWIRT Project (devoted to the search and follow-up of extragalactic SNe in the near-infrared) but also allowing to acquire lightcurves and low-resolution spectra of several types of variable stars (Cepheids, RR-Lyrae, cataclysmic, semiregular, eclipsing and long-period variables) and lightcurves of Active Galactic Nuclei (in the framework of the WEBT Project).

Activities suffered severe stops during the strong earthquakes that hit Central Italy in 2009 and then again in 2016-2017. The camera was finally stopped in 2017 and is currently under dismission.

The lessons learned during this long period have allowed us to identify the points of strength for a refurbishment of the infrared facility, taking into account the necessary tradeoff between the desired performances and the available budget. Generally speaking, replacing SWIRCAM with a new large format cryogenic imaging detector proved to be too expensive and therefore scientifically risky when applied to a 1 m-aperture telescope. Our strategy is therefore focused on a figure of merit based on a format significantly larger than that of SWIRCAM, with an increase in the signal thanks to adaptive optics seeing enhancement techniques, albeit at the cost of reducing the applicable spectral range (in fact limiting photometry to J and H bands only). In addition to that, a possible simplification of the detector management could be very welcome, in particular limiting the cooling to temperatures which are low enough without requiring cryogenic conditions.

All these constraints are met by InGaAs detectors, whose technology has evolved in the last decade in such way to present them as a very interesting option for astronomical observations at near-infrared wavelengths. These detectors are sensitive in the 0.9 – 1.7 μm spectral range, so limiting the photometric acquisitions to the Johnson J,H bands only. In addition, when deeply cooled, their spectral response exhibits a cutoff at long wavelengths which is shorter and shorter, up to preventing almost completely the operation in the H band at cryogenic temperatures.

In spite of these drawbacks, InGaAs detectors offer numerous advantages over traditional infrared detectors: for instance, with respect to detectors based on HgCdTe or InSb substrates, they exhibit an higher quantum efficiency, and comparable dark current values at temperatures higher, some tens of degrees below zero; their readout noise is limited thanks to appropriate readout electronics; and they are commercially available with small pixel sizes (down to 10 μm) and large formats (up to 1280 x 1024) at substantially low costs. InGaAs detectors can therefore operate at higher temperatures compared to other infrared detectors, reducing the need for extensive cooling systems and thus simplifying instrument design and operation, and can acquire images covering rather wide fields-of-view while providing an adequate spatial sampling.

The CI²RCE concept is therefore based on the following facts:

- using a commercial InGaAs detector offering adequate values of dark current and readout noise
- limiting the photometry to J and H broad bands (plus any narrow band within this spectral range)
- covering a wide field of view thanks to larger sensors
- combining the near-infrared acquisitions with Adaptive Optics correction based on visible wavefront sensing, and limited to tip/tilt correction for the 1-m aperture telescope
- exploiting the possibility to acquire images at high framerates (up to ~100 fps) to apply post-processing image reconstruction techniques for bright extended sources like for example Solar System objects.

All these factors contribute to an overall figure of merit, where the disadvantage of the limited spectral coverage is compensated by the wide field-of-view (survey speed) and by the improved spatial resolution. The photometric depth (magnitude limit) is expected to be almost unchanged because the higher background is compensated by an equally increased signal thanks to the PSF enhancement due to the adaptive correction.

Our project takes advantage of the National Recovery and Resilience Plan of the Italian government. This program, based on *NextGenerationEU* funds, includes investments in scientific research, with regards to relationships between research and industry, innovation technologies and revitalization of the territories hit hard by the Covid-19 pandemic.

The CI²RCE design activity started in September 2023. Procurement is in progress at the time this paper is written. Integration, installation and commissioning will be completed by 2026, according to the schedule of the funding program.

3. OPTO-MECHANICAL LAYOUT

Refurbishing the infrared facility based on the SWIRCAM camera means first of all adapting a new imaging sensor to the telescope focal plane where SWIRCAM has worked. The native focal plane scale of 26.04 arcsec/mm resulted in 1.04 arcsec/pix for the SWIRCAM pixel size of 40 µm. When designing SWIRCAM, this was considered enough to sample the seeing PSF, having a typical FWHM of 2.2 arcsec. Placing a new detector with a pixel size of 10 µm would result in a platescale of 0.26 arcsec/pix, with a relevant oversampling of the PSF.

The CI²RCE optical design is therefore based on an optical interface with the telescope which produces a f/# reduction from 7.2 to 6. This choice implies a detector platescale of 0.33 arcsec/pix for a pixel size of 10 and a platescale of 0.50 arcsec/pix for a pixel size of 15 µm. Assuming a reference pixel size of 12 µm, the corresponding sampling for the new detector is 0.375 arcsec/pix. This value is still oversampling a 2.2 arcsec FWHM PSF, without considering however the PSF enhancement due to the tip/tilt correction and the possibility to apply image-restoration techniques. The adaptive correction is indeed expected to produce a corrected PSF with a FWHM down to less than 1.5 arcsec, which will then be sampled with about 4 pixel: such a sampling will leave room, especially in case of planetary studies, for the application of non-real time image restorations techniques, with the possibility to get final images at ~1 arcsec resolution.

The sensor platescale of 0.375 arcsec/pix corresponds to a field-of-view of 8.0 x 6.4 arcmin² for a 1280 x 1024 sensor. The covered sky area, resulting to be 51.2 arcmin², is almost 2.65 times the area covered by the SWIRCAM (19.32 arcmin²).

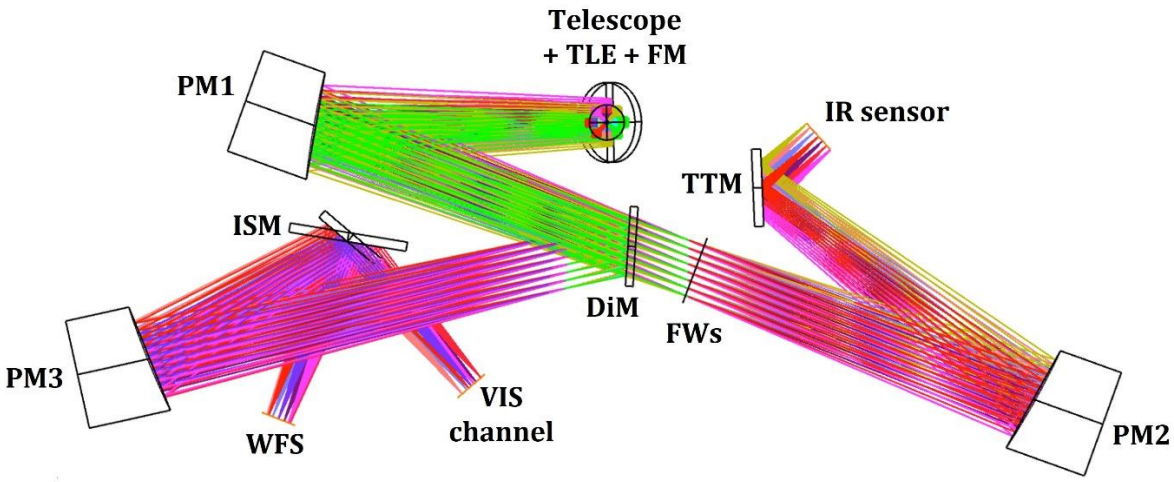


Figure 2. CI²RCE optical layout. The beam from the telescope is collimated by a first off-axis parabolic mirror: out of this VIS/NIR collimated beam, the visible part is picked by a dichroic mirror and redirected toward a tip-tilt sensor. Only the near-infrared part is transmitted, which is refocused onto the near-infrared detector. The exit pupil, after the dichroic, hosts the bandpass filters for photometry and an objective prism for low-resolution imaging spectroscopy.

The optical scheme is reported in Figure 2. The overall path is developed on a plane perpendicular to the output axis of the telescope, via a Folding Mirror (FM) placed just after and optical adapter composed by a Triplet Lens (TLE) mounted into the telescope Cassegrain flange. The optical beam is then collimated by an off-axis Parabolic Mirror (PM1) and finally refocused onto the infrared detector by a second off-axis Parabolic Mirror (PM2).

A Dihroic Mirror (DiM) -placed on the collimated beam, just before the filter wheels- transmits the near-infrared light (0.9 – 1.7 μm range) only, while reflecting its visible part and redirecting it toward a tip/tilt sensor camera (WFS), where the still collimated beam is focused by a third off-axis parabolic mirror (PM3). On this beam, a movable flat mirror acts as an Instrument Selector Mirror (ISM) for an additional instrument port.

Two Filter Wheels (FW) are placed around the exit pupil. Each wheel is planned to host five positions, distributed as reported in Table 1. Worth of notice is the installation of an objective prism, in order to perform very low-resolution spectroscopy or spectrophotometry for targets not too faint.

Table 1. Planned photometric filters and dispersers for imaging photometry and spectroscopy with CI^{2}RCE camera system.

Filter Wheel#1	
Pos#11	Closed
Pos#12	Open
Pos#13	J
Pos#14	H_{short} (cut @ 1.65 μm)
Pos#15	Obj Prism

Filter Wheel#2	
Pos#21	Open
Pos#22	Narrow#1 (λ_C=1.18 μm)
Pos#23	Narrow#2 (λ_C=1.27 μm)
Pos#24	Narrow#3
Pos#25	Narrow#4

The three off-axis parabolas have the same curvature radius and only differ as to the clear aperture. From the manufacturing point of view, this of course represents a great advantage, since all these mirrors will be cut by the same blank.

Finally, the optical system includes a tip/tilt mirror (TTM), placed on the converging beam in front of the infrared sensor, and acting in coordination with the WFS. The possibility to apply a tip/tilt correction came from the experience with similar systems, already prototyped at the time of SWIRCAM, and from the current wide availability of proper devices on the market. The performances of the tip/tilt correction have been simulated starting from the input parameters reported in Table 2 and considering $n_{frame}=10^4$ representations of a point source that is built using $n_{modes}=100$ Zernike modes, weighted using the Noll relations [6].

Table 2. Input data for the tip/tilt correction simulation.

Description	**Symbol**	**Value**
Observational wavelength [m]	λ_{REF}	$1.65 \cdot 10^{-6}$
Seeing [arcsec]	θ	2.2
Resulting Fried radius [m]	r_0	0.15
Aperture diameter [m]	D	1.1
Pixel scale [arcsec/pix] with subsampling	Δx	0.04

The statistics of these random representations is shown in Figure 3, where the Noll coefficients are reported for each Zernike mode, showing the predominance of atmospheric turbulence power in the lowest four orders, i.e. tip/tilt and the third-order aberrations.

The presence of strong aberrations above the tip and tilt is of course related to the telescope aperture. The probability of "a lucky exposure" with SR ≥ 37 % (i.e. a wavefront variance < 1 rad^2 across the aperture diameter D) is given by Fried [7]:

$$P \simeq 5.6 \cdot \exp[-0.1557 \cdot (D/r_0)^2]$$

where r_0 is the Fried parameter. In the case of Campo Imperatore D=1.1 m and, assuming a medium seeing of 2.2 arcsec in H band, we obtain r_0=0.15 m, so that D/r_0 =7.33. This implies that only one image out of ~770 is essentially affected by tip/tilt only and the TT-correction during an acquisition will enhance the PSF only to a limited extent.

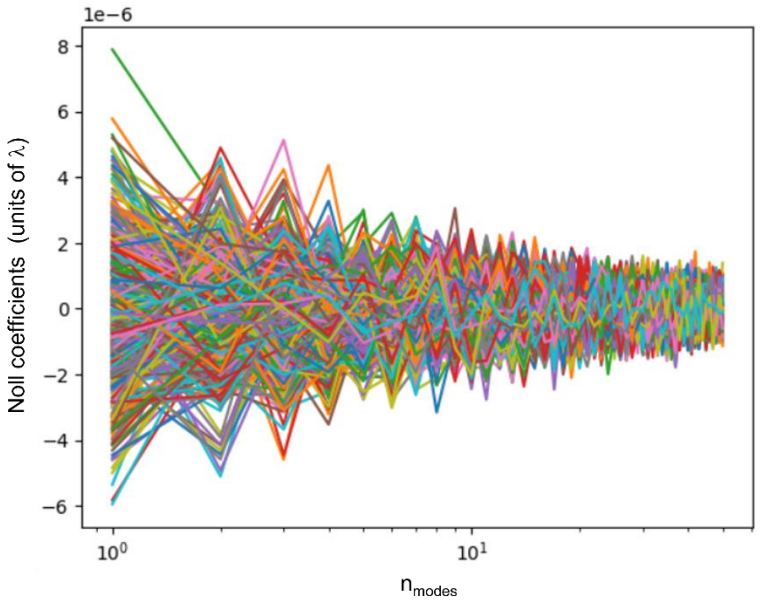


Figure 3. Noll coefficient distribution for turbulence Zernike modes. A very relevant amount of turbulent power is concentrated within the first four modes, i.e. tip/tilt plus third-order aberrations.

However, taking into account that the probability increases if we consider images with SR < 37% , the expected performance of the tip/tilt correction appears very promising as well. Of course the correction works if the WFS exposure time is short enough to freeze the atmospheric turbulence, i.e., shorter than the speckle coherence time T_e related to the ratio of the Fried parameter r_0 to the average wind velocity, v: for the values expected at the Campo Imperatore site, $r_0 \simeq 0.1$ m and v=10 m/s, such exposure time is about 30 ms, i.e. the WFS should work at framerates not less than 35 fps.

The overall results show that the enhancement of the PSF would result, in the majority of cases, in a $\Delta FWHM \sim$ -0.4 arcsec: this means that on average we expect to be able to perform photometric observations at 1.8 arcsec resolution, with a good probability to get imaging at 1.6 arcsec (corresponding to 2.0 arcsec seeing) and, even if rather unfrequent, excellent seeing situations (1.8 arcsec) where TT-corrected images would result to exhibit seeing-limited sources with 1.4 arcsec FWHM.

All these considerations refer to the real-time TT-correction: post-processing image restoration could furtherly improve the spatial resolution, giving the possibility to perform ~1 arcsec resolution imaging, especially for bright targets like Solar System planets and other bodies.

The possibility to work with enhanced seeing has a direct impact on the expected sensitivity, as shown in the next Section.

4. EXPECTED SENSITIVITY

Sensitivity simulations have been carried out taking into account the optical design, the IR sensor characteristics, the overall (telescope+optics) thermal background, the infrared glow due to our atmosphere, and the effect of the tip/tilt correction.

The optical design produces a platescale small enough to reduce the sky background on each pixel in proportion to reduction of sky area per pixel: from 1.04 arcsec to 0.375 arcsec, the sky background hitting the pixel is reduced to $(0.375 / 1.04)^2$ = 13 %, which is particularly relevant for the H band.

Sensor characteristics have been examined: InGaAs sensors, being cooled to just some tens degrees below 0 °C, exhibit a dark current signal incomparably higher than cryogenic detectors. However, simulations performed for the previous SWIRCAM camera showed that the sensitivity was pretty constant for dark current levels much higher than the operational one (0.03 e/s/pixel), and started to worse only for dark rates higher than 30 e/s/pix. This allowed us to develop our concept based on InGaAs sensors, whose dark current can be as low as 80 e/s/pixel at -60 °C and much lower if the detector is cooled down to -80 °C (dark signal nominally is halved every -7 °C cooling).

It has to be considered that InGaAs detectors can be cooled at cryogenic temperatures, but at the cost of losing the H band operability: the spectral response cutoff wavelength, indeed, drops from 1.72 µm at +20 °C to 1.64 µm at -80 °C and again to 1.5 µm below -110 °C. Therefore, for our goals (photometry in J and H bands) we were forced to consider InGaAs with "moderate" cooling (-60 °C ÷ -80 °C) rather than a cryogenic one, even if much less noisy.

When considering the readout noise, the "intrinsic" background budget is of course worsened: it is however largely compensated by the quantum efficiency of InGaAs detectors, higher than 90%, and therefore not comparable with the previous SWIRCAM quantum efficiency, which did not exceed 60 %.

Thermal emission from the telescope and the optics has been modeled, assuming grey-body spectra at different seasonal temperatures of the site and with the emissivity for each material or coating. In general, the instrument thermal background is dominated by the telescope primary mirror, while the optical system gives a small contribution (less than 3%) even at room temperatures. It would be important for the K band, while is still acceptable in the H band and almost negligible in the J band. This behavior is shown in Figure 4 for a set of configurations, considering both the status of the primary mirror (from completely clean to substantially dusty) and the size of the secondary mirror (in the hypothesis of its resizing in the future). The expected thermal background in H allowed us to develop the optomechanical design without the need of cooling the optics, so greatly simplifying it.

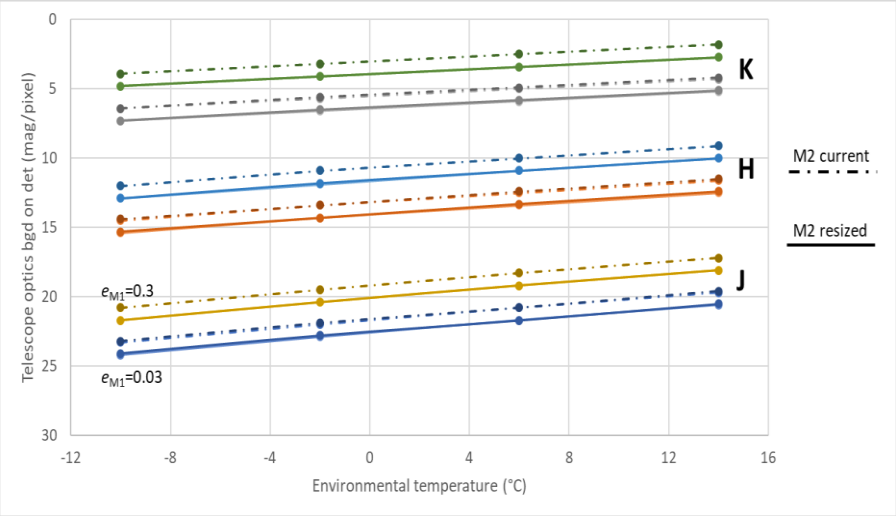


Figure 4. Overall instrumental (telescope + optics) thermal background expected for CI2RCE in the J, H and K bands, at different temperatures of the Campo Imperatore site ranging from -10 °C (winter) to +14 °C (summer). For each band, dash-and-dot lines represent the background onto the detector (in magnitudes/pixel) in the two cases of completely clean primary mirror (emissivity: 3%) or substantially dusty (emissivity: 30%), while continuous lines show the same results in the case the telescope secondary mirror will be resized from the current 590mm to 420mm. The background in K band would require some cooling of the optics: in our case (J and H bands only), the values allowed us to design the opto-mechanical system without active cooling.

Sensitivity computation results are shown in Figures 5, 6 and 7, which report the magnitude-vs-exptime curves for different signal-to-noise ratios. The exposure time is always considered as the sum of a proper number of subexposures.

The effect of the readout noise is clearly visible in Figure 5, where sensitivity in J band are compared in the case of 5 s and 30 s subexposures: the same overall exposure time is indeed reached with a substantially different number of subexposures, each contributing with the readout noise level. The increase by a factor 6 (from 30 s to 5 s) implies a decrease of the observed astronomical signal (at the same signal-to-noise ratio) of almost 1.5 magnitudes. The difference between the two cases, on the other hand, is not a matter of choice, but is determined by the amount of photons (from the observed target plus the sky and instrumental background) with respect to the detector well depth.

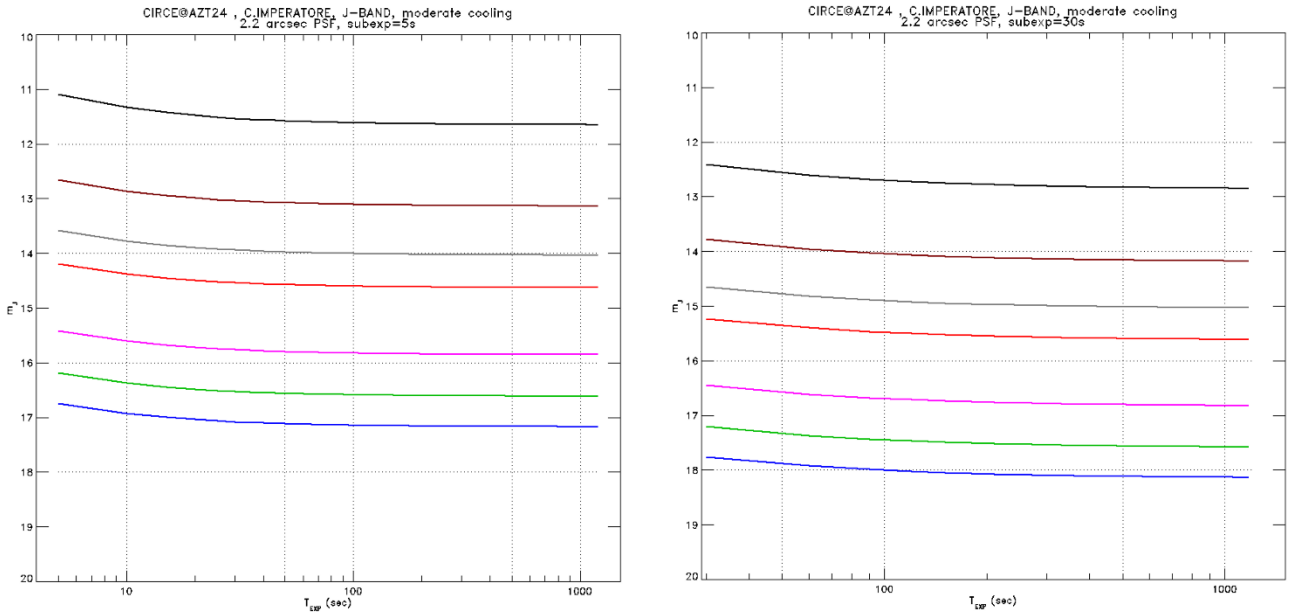


Figure 5. Expected sensitivity for J band and the effect of number of subexposures (i.e. the readout noise). The different colored curves refer to different values of the S/N ratio: from top to bottom, 200, 100, 50, 30, 10, 5, 3.

On the other side, Figure 6 shows the sensitivity improvement given by the tip/tilt correction, in particular with the reduction of the PSF FWHM from 2.2 arcsec to 1.8 arcsec. The same signal-to-noise ratio, in the J band, is obtained for sources about 0.3 magnitudes fainter. The expected improvement is of course larger in exceptionally good conditions (where the tip/tilt correction is expected to produce a FWHM down to 1.4 arcsec and we expect to detect sources 0.6 magnitudes fainter) and possibly after the application of post-processing image reconstruction techniques.

Finally, a comparison between the sensitivity expected in J band (with 30 s subexposure) and H band (with 10 s subexposure), with tip/tilt correction active, is shown: CI^{2}RCE is expected to detect point-like sources down to J=18.1 and H=16.5 with S/N=3.

The sensitivity simulations have to be considered as provisional, and will be continuously updated and refined, especially during the CI^{2}RCE integration in our labs at INAF – Osservatorio Astronomico d'Abruzzo e during its commissioning at the telescope.

The current result allowed us to validate a set of science cases, some of which are described in the next Section.

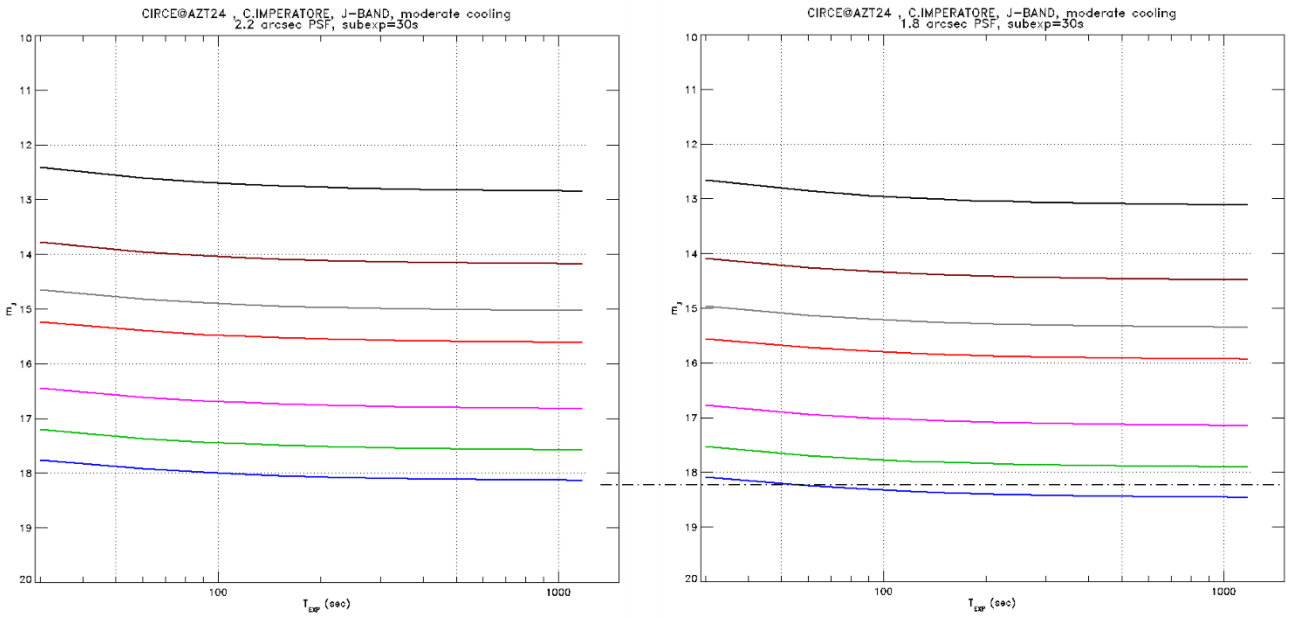


Figure 6. Expected sensitivity for J band and the effect of tip/til correction (i.e. the PSF FWHM). The different colored curves refer to different values of the S/N ratio: from top to bottom, 200, 100, 50, 30, 10, 5, 3.

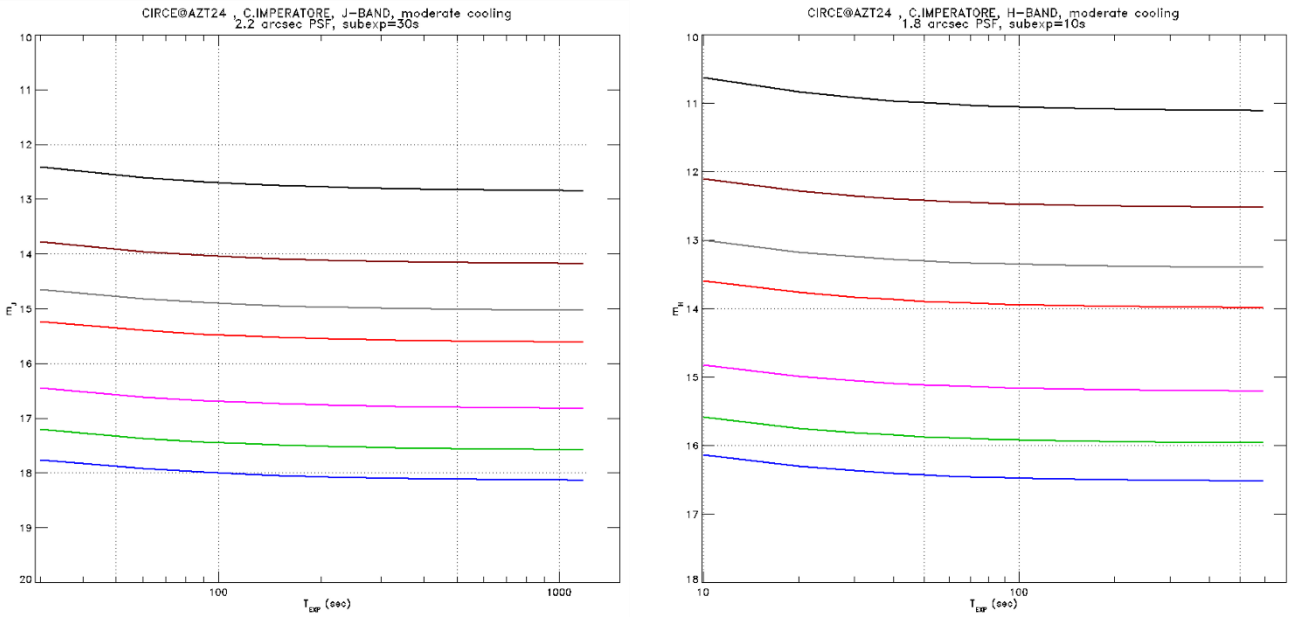


Figure 7. Expected sensitivities for J band (30 sec subexposures) and H band (10 sec subexposures). The different colored curves refer to different values of the S/N ratio: from top to bottom, 200, 100, 50, 30, 10, 5, 3.

5. SCIENCE CASES

A number of science cases have been selected that can be pursued with a 1 m-class telescope equipped with instrumentation for J and H bands photometry. These science cases are directly related to programs pursued with large ground-based

facilities or space-borne telescopes and instruments, to which the access is limited by the large number of requests and the allocated observing time is, in general, not adequate to perform survey or follow-up campaigns.
We report three of them in the following, addressing stellar astrophysics, planetary studies and extragalactic astronomy.

The Cepheid Population of the Milky Way and their use as distance indicators and population tracers

Classical Cepheids (also known as delta Cephei stars, type I Cepheids or population I Cepheids) are among the most famous variable stars. Precisely calibrating the Cepheids Period-Luminosity (PL) and Period-Wesenheit (PW) relation (that is the reddening free formulation of the PL relation) is of paramount importance to cosmology, given its common application to the extragalactic distance scale. Cepheid distances are used as a means of calibrating type-Ia supernovae to measure the Hubble constant (H0), as, for example, by the HST Key Project [8] and subsequently by the SH0ES Project (NIR observations of cepheids in galaxies hosting type-Ia supernovae [9]). Uncertainties in distances to the closest galaxies propagate to further Cepheid-based distance measurements, and in an era ambitiously aiming for accuracies of 1% in H0 [10], minimizing these uncertainties is essential.

A major improvement of the extragalactic distance ladder built by the SH0ES project (NIR observations of Cepheids in galaxies hosting also Type Ia supernovae [11]) has been the photometric homogeneity of Cepheid observations carried out exclusively in the Hubble Space Telescope (HST) photometric system. With the release of time-series observations in Gaia DR3, there is now an additional data set of very high quality, well-resolved multichromatic observations based on a well-characterized and homogeneous photometric system. However the errors underlying the Cepheids PL relation as derived from Gaia DR3 parallaxes still push the global error to the LMC distance to 4.4%. This is partially due to the Gaia parallax systematics that are known to depend on its sky position as well as its magnitude and color [12], as well as to the effect of metallicity on Cepheid luminosity.

Very recently Reyes & Anderson [13] carried out a systematic search for MW clusters Cepheids using Gaia EDR3 and DR3 data and found a clear trend in the comparison between individual and cluster average parallaxes, showing that cluster Cepheids can play a crucial role for the measurement of H0 by providing the best accurate absolute trigonometric scale based on Gaia astrometry. Future developments, such as high-quality photometry of MW Cepheids in and out of clusters will particularly improve the base calibration of the distance scale toward a 1% Hubble constant measurement.

Cepheids are also important astrophysical objects for stellar evolution and Galactic studies. Indeed, since their pulsational properties (mainly periods) are linked to the intrinsic stellar parameters (effective temperature, mass, luminosity) they can be used as an independent test for stellar evolution models. Moreover, given their young age (~50-500 Myr) they are preferentially located in the Milky Way (MW) thin disc, and, thanks to precise distances that can be derived from their PL and PW relations, Cepheids can be used to model the disc and trace their birthplaces in the spiral arms, where star formation is most active.

The near-infrared (NIR) bands undoubtedly offer several advantages on the optical bands: optical-NIR PW relations are minimally affected by uncertainties on the adopted reddening law, and also marginally affected by metallicity effects [14]. This is of particular importance, since the reddening law is different for different galaxies and the effect of the metallicity on the PL and PW is still debated. Moreover the NIR PW relations are linear over the entire period range and, because they mimic period–luminosity–color relations, they have a smaller intrinsic dispersion caused by the width in temperature (color) of the Cepheid Instability Strip (IS). Inno and others [15] used theoretical models to quantify the dispersion due to the width of the IS and showed that NIR PW relations have smaller intrinsic dispersions when compared to optical and optical-NIR ones: in particular, the PW_{JH} and PW_{HJK} relations show the smallest dispersions, which are two–three times smaller than the one found around the PW_{VI} relation. Finally, the frequently high reddening of the cepheids in the MW leads to prefer NIR bands to the optical ones.

Close attention has to be paid to the choice of the objects to be observed in order to minimize the photometric errors. The variables will therefore have to be quite bright and with the presence in the same field of view of calibrators from the 2MASS survey. The number of phase points will have to guarantee a good coverage of the light curve for an accurate mean magnitude (quite easily achievable since the periods are known) and the instrumental effects that can affect an accurate computation of photometry (fringing, detected signal depending on the position on the chip etc) will have to be well known and calibratable.

The list of new variables observed by Gaia [16] and released in DR3, about 200, is a good sample of objects that deserve new NIR observations. By cross-matching the new positions of Gaia with the 2MASS catalog we obtain a list of more than 100 objects observable with CI^2RCE, whose color-magnitude diagram in JH bands is shown in Figure 8.

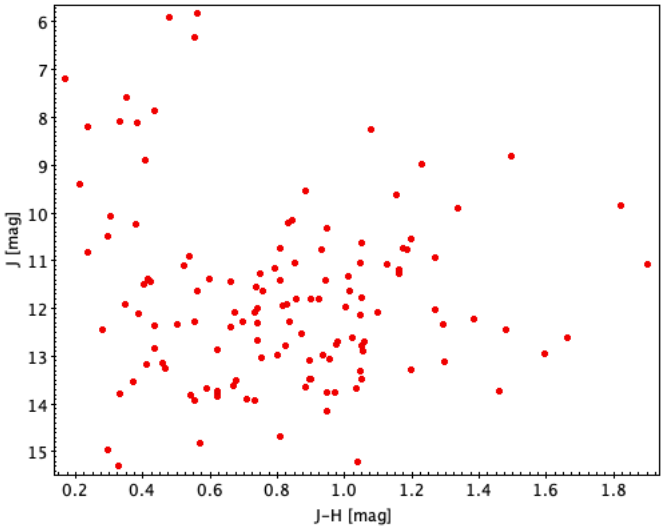


Figure 8. Color-Magnitude Diagram (J vs J-H) of the new cepheids discovered by Gaia that will be observable with CI^{2}RCE. Near Infrared data from 2MASS.

Near-Infrared monitoring of the Night O_2 Airglows in the Venus atmosphere

The thick atmosphere of Venus presents a puzzling and complex dynamic structure. While the cloud layer (approximately from 50 to 70 km altitude) can be thoroughly studied using cloud images in UV, visible and IR [17], the region from 80 to 120 km largely remains a mystery. It neither has clouds to allow motion tracking, nor it is possible to measure winds using in situ probes due to engineering constraints. Yet this region is important for Venus atmospheric dynamics because there occurs the transition from the global retrograde zonal super-rotation (RZS) mode below to the subsolar-antisolar (SS-AS) cell circulation above [18].

However, this transition region can be studied using nightside airglows — NO and O_2, which peak at 110 and 97 km, and can be observed in UV and near-IR (Figure 9) respectively [19][20]. Of particular relevance in this context are infrared observations of the O_2 ($a^1\Delta g$) emission at 1.27 μm wavelength. The atomic oxygen forms on the dayside from the dissociation of CO_2 and then travels to the nightside with the SS-AS circulation where it recombines in the downwelling flow and emits around midnight [21]. However, the maximum of the emission is not found directly at the antisolar point, but shifted towards 22 h of local time. Therefore, other dynamic mechanisms such as thermal tides and stationary gravity waves are suspected to play a role at these altitudes [22].

A significant problem with these results is the lack of experimental data, as only Venus Express spacecraft studied this phenomenon as well as a few short ground-based observations. This issue could therefore be addressed by a new series of ground-based observations of the oxygen nightglow on Venus using CI^{2}RCE. This would provide a unique opportunity to anticipate and complement the wealth of data and studies from the recently selected missions to Venus [23][24][25][26][27][28], opening the possibility to include CI^{2}RCE in the ground segment for the future missions to Venus.

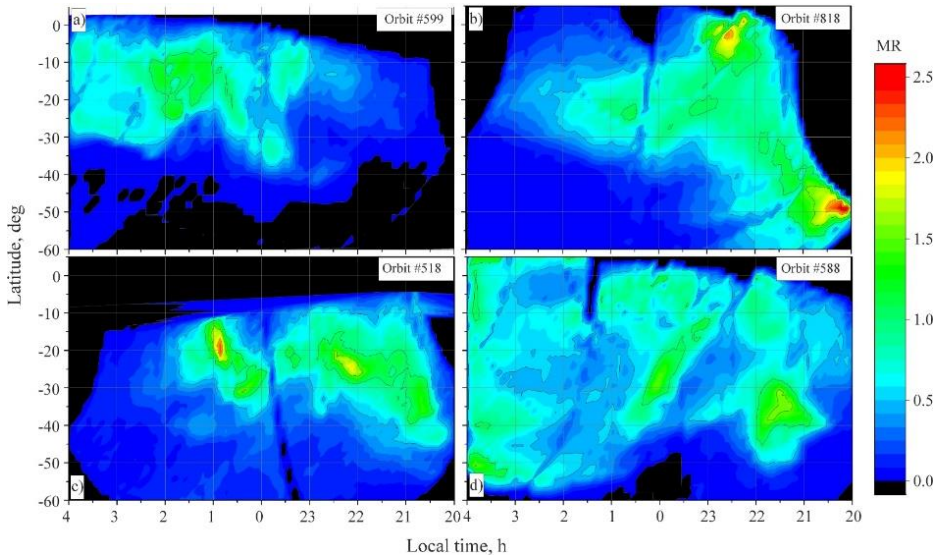


Figure 9. Examples of O_2 ($a^1\Delta g$) airglow emission on Venus nightside in local time—latitude coordinates. Emission intensity is calculated after removing the input of the lower atmosphere and surface, cloud scattering and water vapor absorption: (a) orbit 599 (images 00-07): peak emission is at 1–2 h, most of the bright areas are located on the morning side; (b) orbit 818 (images 00-10): two maxima on the evening side, one of which is near the equator, the other one is in the middle latitudes; (c) orbit 518 (images 00- 01): two maxima on both sides of the midnight meridian; the stronger (but also more spatially compact) one is at 1 h, the weaker (but more extended) one is at 22 h; (d) orbit 588 (images 00-06): several local maxima at 22.5, 0 and 3–4 h LT (from Shakun and others [20]).

Extragalactic transients in the survey Era

Transients are astronomical objects whose luminosity varies over a relatively short time (e.g., weeks to months). While common Galactic transients include cataclysmic variables, eclipsing binaries and transiting exoplanets, extragalactic ones are generally produced by stellar outbursts, mergers and supernova (SN) explosions with peak luminosities above those of the brightest novae ($>10^{38}$ erg s^{-1} [29]).

Late infrared excesses (IR rebrightening) are common in transients, particularly those showing signatures of interaction between ejecta and a pre-existing circumstellar medium. Their origin is still debated and interpretations include light echoes or reprocessing of light from pre-existing dust and absorption/reprocessing of the transient light by newly formed dust in the ejecta. Their proper interpretation is crucial in understanding how dust grains form and the nature of the progenitors (e.g., intermediate-mass, or more massive Wolf-Rayet stars). The modelling of IR emission requires long-term and sufficiently high-cadenced observations in the widest possible infrared range, with near infrared playing an important role in estimating the proper bolometric luminosity of the transient (see [30]). IR re-brightenings have also been observed in tidal disruption events (TDEs; see [31] for a recent review), transients occurring when a star approaches a supermassive black hole (BH) resulting in its complete disruption due to tidal forces. Monitoring these transients at IR wavelengths is therefore crucial also for research related to multi-messenger astronomy.

Many transients suffer heavy interstellar extinction at visible wavelengths, as has been clear with the discovery of SNe in nearby galaxies by optical surveys (see e.g. [32]) or using infrared facilities [33][34]. Stellar evolution models predict that massive stars rapidly end their lives in a core-collapse SN in a relatively short time [35]. The progenitors of these core-collapse SNe are therefore primarily expected in active star-forming regions, where reddening is measured to be as high as 14–25 mag in optical bands. Discoveries of optical surveys may therefore significantly underestimate the true core-collapse SN rates [36].

The crucial importance of multiwavelength observations of transients is therefore quite evident. In particular, NIR observations are crucial to fill the gaps between optical and mid-IR bands provided by ground- and space-based facilities: ideally, JHK observations would be required in order to efficiently cover the 1100-2200 nm range, but even JH bands may provide crucial information to detect the onset of possible IR re-brightenings due to dust emission (light echoes or

absorption due to newly formed dust) or to detect heavily extinguished transients. However, in spite of this, NIR data are often not considered by ongoing surveys (not even in the z-band): systematic follow-up campaigns are largely limited to the number of available ground-based facilities and to the high cost in terms of required telescope time, so that any new NIR facility may give an enormous contribution to this research.

6. A WORK IN PROGRESS…

The project described in this paper is currently running. We plan however to have the infrared system and part of the optical system camera in our laboratories at INAF – Osservatorio Astronomico d'Abruzzo by 2024 fall. The time schedule, determined by the funding program, is rather tight and is reported as follows:

- 2024 Q3-Q4: procurement of CI^{2}RCE subsystems completed
- 2025 Q1-Q3: CI^{2}RCE laboratory integration
- 2025 Q4: installation at the telescope in Campo Imperatore
- 2026 Q1: CI^{2}RCE on-sky commissioning – *Completion of reporting to the EU funding program*
- 2026 Q2: starting CI^{2}RCE operation

ACKNOWLEDGEMENTS

This work is supported by the Italian Government, through the Piano Nazionale di Ripresa e Resilienza (PNRR), based on *NextGenerationEU* funds.

REFERENCES

[1] Rieke, G. H., "Infrared Detector Arrays for Astronomy", Annual Review of Astronomy & Astrophysics, 45 (1), 77, 2007
[2] Sullivan, P. W. et al., "Near-Infrared InGaAs Detectors for Background-limited Imaging and Photometry", Proc. SPIE, 9154, High Energy, Optical, and Infrared Detectors for Astronomy VI, 91541F (2014)
[3] Batty, K. et al., "Laboratory and On-sky Testing of an InGaAs Detector for Infrared Imaging", PASP, 134, 065001 (2022)
[4] Birch, M. et al., "InGaAs focal plane array for transient astronomy in the NIR", J. Astron. Telesc. Instrum. Syst., 8 (1), 016001-1 (2022)
[5] D'Alessio, F. et al., "SWIRCAM: a NIR imager-spectrometer to search for extragalactic supernovae", Proc. SPIE, 4008, Optical and IR Telescope Instrumentation and Detectors, 748 (2000)
[6] Noll, R. J., "Zernike polynomials and atmospheric turbulence", Optical Society of America Journal, 66, 207 (1976)
[7] Fried, D. L., "Probability of getting a lucky short-exposure image through turbulence",Optical Society of America Journal, 68, 165 (1978)
[8] Freedman, W. L. et al., "Final Results from the Hubble Space Telescope Key Project to Measure the Hubble Constant", Astrophys. J., 553 (1), 47 (2001)
[9] Riess, A. G. et al., "Large Magellanic Cloud Cepheid Standards Provide a 1% Foundation for the Determination of the Hubble Constant and Stronger Evidence for Physics beyond ΛCDM", Astrophys. J., 876 (1), 85 (2019)
[10] Riess, A. G. et al., "Cosmic Distances Calibrated to 1% Precision with Gaia EDR3 Parallaxes and Hubble Space Telescope Photometry of 75 Milky Way Cepheids Confirm Tension with ΛCDM", Astrophys. J. Lett., 908 (1), L6 (2021)
[11] Riess, A. G. et al., "A Comprehensive Measurement of the Local Value of the Hubble Constant with 1 km s-1 Mpc-1 Uncertainty from the Hubble Space Telescope and the SH0ES Team", The Astrophys. J. Lett., 934 (1), LD7 (2022)
[12] Lindegren, L., et al., "Gaia Early Data Release 3. Parallax bias versus magnitude, colour, and position", Astron. Astrophys., 649, A4 (2021)
[13] Reyes, M. C. and Anderson, R. I., "A 0.9% calibration of the Galactic Cepheid luminosity scale based on Gaia DR3 data of open clusters and Cepheids", Astron. Astrophys., 672, A85 (2023)

[14] Inno, L., et al., “On the Distance of the Magellanic Clouds using Cepheid NIR and Optical–NIR Period–Wesenheit Relations”, Astrophys. J., 764 (1), 84 (2013)
[15] Inno, L., et al., “The Panchromatic View of the Magellanic Clouds from Classical Cepheids. I. Distance, Reddening, and Geometry of the Large Magellanic Cloud Disk”, Astrophys. J., 832 (2), 176 (2016)
[16] Ripepi, V., et al., “Gaia Data Release 3. Specific processing and validation of all sky RR Lyrae and Cepheid stars: The Cepheid sample”, Astron. Astrophys., 674, A17 (2023)
[17] Peralta, J., et al., “Overview of useful spectral regions for Venus: An update to encourage observations complementary to the Akatsuki mission”, Icarus, 288, 235 (2017)
[18] Bougher, S.W., Alexander, M. J. and Mayr, H. G., “Upper Atmosphere Dynamics: Global Circulation and Gravity Waves”, in: Venus II : Geology, Geophysics, Atmosphere, and Solar Wind Environment. Edited by Stephen W. Bougher, D.M. Hunten, and R.J. Philips. Tucson, AZ : University of Arizona Press, p.259 (1997)
[19] Stiepen, A., et al., “The vertical distribution of the Venus NO nightglow: Limb profiles inversion and one-dimensional modeling”, Icarus, 220 (2), 981 (2012)
[20] Shakun, A. V., et al., “O_2 ($a^1\Delta g$) Airglow at 1.27 μM and upper Mesosphere Dynamics on the Night Side of Venus”, Solar System Research, 57 (3), 200 (2023)
[21] Gérard, J.-C., et al., “Distribution of the O_2 infrared nightglow observed with VIRTIS on board Venus Express”, Geophys. Res. Lett., 35 (2), L02207 (2008)
[22] Gorinov, D., et al., “Circulation of Venusian Atmosphere at 90-110 km Based on Apparent Motions of the O_2 1.27 μm Nightglow From VIRTIS-M (Venus Express) Data”, Geophys. Res. Lett., 45 (5), 2554 (2018)
[23] Garvin, J. B., et al., “Revealing the Mysteries of Venus: The DAVINCI Mission”, Planetary Science J., 3 (5), 117 (2022)
[24] Zasova, L. V., et al., “Venera-D: A Design of an Automatic Space Station for Venus Exploration”, Solar System Research, 53 (7), 506 (2020)
[25] Senske, D., et al., “The Venera-D Mission Concept, Report on the Activities of the Joint Science Definition Team”, in: 15th Meeting of the Venus Exploration and Analysis Group (VEXAG), held 14-16 November, 2017 in Laurel, Maryland. LPI Contribution No. 2061, p.8014 (2017)
[26] Ghail, R., et al., “EnVision Assessment Study Report, Yellow Book” (2021)
[27] Haider, S. A., et al., “Indian Mars and Venus Missions: Science and Exploration”, 42nd COSPAR Scientific Assembly. Held 14-22 July 2018, in Pasadena, California, USA, Abstract id. B4.1-10-18 (2018)
[28] Smrekar, S., et al., “VERITAS (Venus Emissivity, Radio Science, InSAR, Topography And Spectroscopy): A Proposed Discovery Mission”, 14th Europlanet Science Congress 2020, held virtually, 21 September 2020 - 9 October, 2020 (2020)
[29] Pastorello, A. and Fraser, M., “Supernova impostors and other gap transients”, Nature Astronomy, 3, 676 (2019)
[30] Tartaglia, L., et al., “SN 2018ijp: the explosion of a stripped-envelope star within a dense H-rich shell?”, Astron. Astrophys., 650, A174 (2021)
[31] Gezari, S., “Tidal Disruption Events”, Ann. Rev. Astron. Astrophys., 59, 21 (2021)
[32] Tartaglia, L., et al., “The Early Detection and Follow-up of the Highly Obscured Type II Supernova 2016ija/DLT16am”, Astrophy. J., 853 (1), ID62 (2018)
[33] Di Paola, A., et al., “Discovery of the heavily obscured supernova 2002cv”, Astron. Astrophys., 393, L21 (2002)
[34] Kankare, E., et al., “Discovery of a Very Highly Extinguished Supernova in a Luminous Infrared Galaxy”, Astrophys. J. Lett., 689 (2), L97 (2008)
[35] Schaller, G., et al., “New Grids of Stellar Models from 0.8-SOLAR-MASS to 120-SOLAR-MASSES at Z=0.020 and Z=0.001”, Astron. Astrophys. Suppl., 96 (2), 269 (1992)
[36] Mattila, S., Meikle, W. P. S. and Greimel, R., “Highly extinguished supernovae in the nuclear regions of starburst galaxies”, New Astron. Rev., 48 (7-8), 595 (2004)